Effect of source spectral shape on task-based assessment of detection and resolution in optical coherence tomography

A. Ceyhun Akcay, Eric Clarkson, and Jannick P. Rolland

We demonstrate the effect of the spectral shape of broadband light sources in a task-based approach for assessment of signal detection and resolution in optical coherence tomography. We define two binary tasks: The signal is either present or absent and the signal can be either resolved or not. In a transparent sample bounded by two uniform interfaces we study the minimum detectable change in the index of refraction as well as the minimum resolvable distance between the layers in correlation with the source spectral shape and power. Results show that the area under the receiver operating curve (AUC) for a signal-detection task is not affected by the shape of the spectrum but solely by its optical power, whereas spectral shaping has an effect, which we quantify, on the AUC for the resolution task. Moreover, the AUC is demonstrated in relation to the concept of system sensitivity for a signal-detection task.   © 2005 Optical Society of America

OCIS codes: 000.5490, 030.6600, 170.4500.

1. Introduction

Optical coherence tomography[1] (OCT) is an interferometric biomedical imaging technique based on the temporal coherence property of a broadband light source that is used to generate cross-sectional images of biological tissues at high axial resolution. The axial resolution of the imaging system is often described by the point-spread function of the imaging system, which is defined as the envelope of an interference signal formed by varying the optical path length in the sample or reference arm, that is, scanning a scattering or reflecting point object throughout the depth of focus in the specimen, i.e., the sample.[2] We previously quantified the effect of change in source spectral shape on axial resolution[3] and then demonstrated how to improve the point-spread function of an OCT system by shaping the source power spectrum.[4]

A. C. Akcay and J. P. Rolland (jannick@odalab.ucf.edu) are with the College of Optics and Photonics, CREOL, and the Florida Photonics Center of Excellence, University of Central Florida, Orlando, Florida 32816. E. Clarkson is with the Optical Science Center, Department of Radiology, University of Arizona, Tucson, Arizona 85720.

Recently we developed a mathematical framework based on task performance that uses statistical decision theory for the optimization and assessment of OCT.[5] The development of such a framework was motivated by the art of diagnosis in medical imaging, in which image quality is estimated based on the performance of an observer on specific tasks.[6] Assessing the image quality provided by an imaging system without a given task and based on the observer's opinion is called subjective assessment. Subjective assessment provides arguable results as it may change with the system or observer and it does not fulfill a purpose.[7] Therefore a definition of task is necessary for objective assessment. Two major task categories may be defined: classification and estimation. We define two tasks for an OCT signal or image: a signal-detection task and a resolution task. A signal-detection task is generated to investigate whether the OCT signal can be detected. The purpose of a resolution task is to study whether two interfaces or features can be resolved with the OCT system.[5]

In this paper, we apply such a framework to analyze the effect of the source spectral shape on two tasks, a signal-detection task and a resolution task. Such tasks are binary classification tasks since they each consist of only two hypotheses, which are the negative hypothesis H_0 and the positive hypothesis H_1. We have two classes defined for these tasks: the zeroth class for the cases when H_0 is true and the first

class for the cases when H_1 is true. Different types of observer models have been described and discussed in the literature.[5,7–10] An ideal observer can be employed to perform the task if all statistical information of the data is available to the observer, i.e., a probability density function (PDF) is known under each hypothesis. The ideal observer provides the maximum performance one can get from any observer. When the PDF information is not available, the Hotelling observer[8] is a preferred alternative. The Hotelling observer is a linear discriminant that depends on the second-order statistics of the data. In this paper, we employ the Hotelling observer to perform the defined classification tasks. The Hotelling observer generates a scalar detectability index[5] to discriminate data into the given classes according to the negative and positive hypotheses. In Ref. 5 we proposed to use the detectability index and the area under the receiver operating characteristics curve (AUC) to determine how well an optical coherence imaging system, which we considered a free-space Michelson interferometer, performs a given task. We thereafter investigated the change in the performance of the Hotelling observer on the detection and resolution tasks when the source power spectrum is smoothed by optical spectral shaping.

2. Mathematical Model

We can represent any object data, i.e., signal or image, as an $N \times 1$ column vector **I**, which is in our case a set of photocurrent signal $I(t)$ acquired and sampled at the output of the OCT photodetector. The detectability index, or effective signal-to-noise-ratio (SNR), associated with the performance of the Hotelling observer is given by

$$d^2 = \mathbf{X}^{\dagger}\mathbf{K}^{-1}\mathbf{X}, \qquad (1)$$

where **X** is an $N \times 1$ column vector representing the difference in the ensemble-averaged vectors of the two classes of binary classification task for hypothesis H_0 and hypothesis H_1 and † denotes the transpose and complex conjugate. If the detected photocurrent signal supports hypothesis H_0, then it belongs to the zeroth class and the signal vector is denoted by $\mathbf{I}_0$. Similarly, if the photocurrent signal indicates that hypothesis H_1 is true, we denote the signal vector by $\mathbf{I}_1$. Hence vector **X** will be given by

$$\mathbf{X} = \langle \mathbf{I}_1 \rangle - \langle \mathbf{I}_0 \rangle, \qquad (2)$$

where $\langle \rangle$ indicates the ensemble average over all sources of randomness. The quantity **K** in Eq. (1) is an $N \times N$ matrix that represents the weighted-average covariance matrices across the two classes based on their *a priori* probability. If we assume that the probability of occurrence of each class is the same, i.e., one half, then **K** will be given by

$$\mathbf{K} = \frac{1}{2}(\mathbf{K}_1 + \mathbf{K}_0), \qquad (3)$$

where $\mathbf{K}_i$ are the autocovariance matrices under each class (i.e., $i = 0, \ 1$). The elements of the autocovariance matrix may be written as

$$K_i(t_n, \ t_m) = \langle I_i(t_n)I_i(t_m) \rangle - \langle I_i(t_n) \rangle \langle I_i(t_m) \rangle. \qquad (4)$$

The Hotelling observer makes a decision by taking the inner product of a template vector with the data vector and comparing the resulting scalar with a threshold. The Hotelling template is the product of the inverse of the average covariance matrix **K** with the vector **X** presented. This template maximizes the effective SNR of the resulting test statistic, and the resulting maximal effective SNR is called the Hotelling trace. Unlike the conventional concept of sensitivity of an OCT signal,[11–13] in which the sensitivity corresponds to the SNR obtainable with a 100% reflective sample and provides a measure for minimum detectable sample reflectivity,[13] the detectability index or effective SNR is a measure of separability of the classes that comprise an ensemble of images spanning various instances of the noise. The separability is determined by the ratio between the distance of the ensemble averages of each class, i.e., the difference between them, and scatter around the ensemble averages of each class. Such a detectability index complements the conventional concept of sensitivity by providing a statistical approach to the classification of data, i.e., assignment of a signal to a certain class around the limit of detectable minimum reflectivity, given that the classification of noisy data sets is a stochastic process.

We can relate the detectability index to a common scalar quantity called the AUC, under the assumption that the Hotelling test statistic is normally distributed under each class.[6,8] This normality assumption can be justified under the central limit theorem since the Hotelling test statistic is a linear combination of the components of the data vector and, for the task we are considering, these components are statistically independent random variables. The AUC relation is given by

$$\mathrm{AUC} = \frac{1}{2} + \frac{1}{2} \ \mathrm{erf}\left(\frac{\sqrt{d^2}}{2}\right), \qquad (5)$$

where erf( ) is the error function. The AUC is a common figure of merit for task performance. The value of the AUC changes between 0.5 and 1, as indicated in Eq. (5). The AUC represents the probability of correct discrimination when a test datum is evaluated to determine whether it belongs to a certain class (0 or 1). An AUC value of 0.5 means that the discrimination of classes is not possible, while an AUC value of 1 corresponds to a perfect discrimination.

3. Photocurrent Signal

A well-known characteristic of light sources employed in OCT imaging is the broadness of their

spectral bandwidth. The electric field emitted by the source consists of multiple plane waves with different angular optical frequencies in the spectral band of the source power spectrum. Hence the source electric field $\mathbf{E}_{so}(t)$ can be expressed as the sum of its Fourier components as

$$\mathbf{E}_{so}(t) = \int_{-\infty}^{\infty} \exp(i\omega t) \, \hat{\mathbf{E}}_{so}(\omega) \, \mathrm{d}\omega, \qquad (6)$$

where the caret ($\wedge$) denotes a Fourier domain function and boldface variables are vector or matrix quantities. The angular optical frequency ω equals $2\pi\nu$, where ν is the optical frequency. In a Michelson interferometer, which is the common setup used for optical coherence imaging, the amplitude of the source electric field is split at the beam splitter and directed into a reference arm and a sample arm of the interferometer. We can describe the losses as being due to the beam splitter, the absorption in the interferometer arms, nonequal reflection from the reference mirror and sample mirror, or a sample as a frequency-dependent function as $\hat{\alpha}_r(\omega)$ for the field propagating in the reference arm and as $\hat{\alpha}_s(\omega)$ for the field propagating in the sample arm. Therefore, the expression for the electric field at the photodetector, which consists of the electric fields recombined at the beam splitter, can be given by

$$\mathbf{E}(t) = \int_{-\infty}^{\infty} \{\hat{\alpha}_r(\omega) \, \exp[i\phi_r(\omega, \ t) + i\omega t]$$
$$+ \hat{\alpha}_s(\omega) \, \exp[i\phi_s(\omega, \ t) + i\omega t]\} \, \hat{\mathbf{E}}_{so}(\omega)\mathrm{d}\omega, \quad (7)$$

where $\phi_r(\omega)$ and $\phi_s(\omega)$ are the phases accumulated through propagation in the reference and sample arms of the interferometer, respectively. We represent the expression in curly brackets { } in Eq. (7) as $m(\omega, \ t)$ for the sake of simplicity.

The photocurrent signal $I(t)$ generated at the photodetector is related to the number of photoelectrons $N(t)$ induced by the incident electric field over the integration time of the photodetector Δt. We know that the creation of photoelectrons obeys Poisson statistics, whereas the electric field emitted by the broadband light source presents characteristics of circular Gaussian statistics with $\langle \mathbf{E}(t) \rangle$ equal to zero.[14] Because the photodetector provides a mean photocurrent at the output, the relation between the output photocurrent and the number of photoelectrons is given by

$$\langle\langle I(t) \rangle\rangle = \left\langle \left\langle \frac{e}{\Delta t} \int_{-\infty}^{\infty} r(t - t')N(t')\mathrm{d}t' \right\rangle \right\rangle$$
$$= \frac{e}{\Delta t} \int_{-\infty}^{\infty} r(t - t')\langle\langle N(t') \rangle\rangle \mathrm{d}t', \qquad (8)$$

where e is the charge of an electron (1.6×10^{-19} C), the double angle brackets represent statistical averaging over both random processes, and $r(t)$ is the integration time window of the photodetector given by

$$r(t) = \begin{cases} 1, & 0 \le t \le \Delta t \\ 0, & \text{otherwise} \end{cases}. \qquad (9)$$

The mean number of photoelectrons $\langle\langle N(t) \rangle\rangle$, indicating averaging over both the Poisson noise associated with detection and the Gaussian noise associated with the source field, is defined as $\rho\langle \mathbf{E}^{\dagger}(t)\mathbf{E}(t) \rangle$, where ρ is given by $RA/(e\eta_0)$, where R and A are the responsivity and area of the detector, respectively, and η_0 is the impedance of free space (377 Ω). The detector responsivity R, which is a function of optical frequency, is assumed to be unity for all frequencies. From Eq. (7) we derive the mean number of photoelectrons as

$$\langle\langle N(t) \rangle\rangle = \rho \int_{-\infty}^{\infty} \int_{-\infty}^{\infty} m^*(\omega, \ t)m(\omega', \ t) \, \exp[i(\omega' - \omega)t]$$
$$\times \langle \hat{\mathbf{E}}_{so}^{\dagger}(\omega)\hat{\mathbf{E}}_{so}(\omega') \rangle \, \mathrm{d}\omega \, \mathrm{d}\omega', \qquad (10)$$

where * denotes the complex conjugate. Assuming that the source field is a stationary random process, we can express $\langle \hat{\mathbf{E}}_{so}^{\dagger}(\omega)\hat{\mathbf{E}}_{so}(\omega') \rangle$ in terms of the source power spectrum $S(\omega)$ as[5,14,15]

$$\langle \hat{\mathbf{E}}_{so}^{\dagger}(\omega)\hat{\mathbf{E}}_{so}(\omega') \rangle = \delta(\omega - \omega')S(\omega). \qquad (11)$$

When Eq. (11) is inserted into Eq. (10), the mean photocurrent in Eq. (8) becomes

$$\langle\langle I(t) \rangle\rangle = \frac{\rho e}{\Delta t} \int_{-\infty}^{\infty} r(t - t')$$
$$\times \left[\int_{-\infty}^{\infty} |m(\omega, \ t')|^2 \, S(\omega)\mathrm{d}\omega \right] \mathrm{d}t', \quad (12)$$

where

$$|m(\omega, \ t')|^2 = |\hat{\alpha}_r(\omega)|^2 + |\hat{\alpha}_s(\omega)|^2$$
$$+ 2 \, \mathrm{Re} \, \{\hat{\alpha}_r^*(\omega)\hat{\alpha}_s(\omega) \, \exp[-i\phi_r(\omega, \ t')$$
$$+ i\phi_s(\omega, \ t')]\}. \qquad (13)$$

Inserting Eq. (11) into Eq. (10) yields

$$\langle\langle N(t) \rangle\rangle = \rho \int_{-\infty}^{\infty} |m(\omega, \ t)|^2 \, S\omega \, \mathrm{d}\omega. \qquad (14)$$

4. Evaluation of the Hotelling Observer Performance

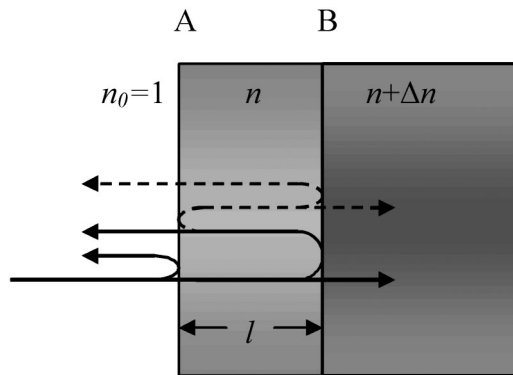We described in the previous section the basics on how to quantify the performance of a Hotelling ob-

Fig. 1. Sample model: n is the refractive index of the sample and Δn is the change of refractive index from sample to substrate.

server by computing the associated detectability index and AUC. Given the two sources of randomness in the system together with Eq. (1) for the mean photocurrent, the sampled autocovariance matrix elements shown in Eq. (4) should be updated as

$$K_i(t_n,\ t_m) = \langle\langle I_i(t_n)I_i(t_m)\rangle\rangle - \langle\langle I_i(t_n)\rangle\rangle\langle\langle I_i(t_m)\rangle\rangle.$$
(15)

A more explicit expression for the autocovariance matrix elements for the ith class is needed to simulate the detectability index and AUC for a task. Such an expression is given by[5]

$$K_i(t_n,\ t_m) \approx \left(\frac{e}{\Delta t}\right)^2 \int_{-\infty}^{\infty} r(t_n - t')r(t_m - t')\langle\langle N_i(t')\rangle\rangle \ \mathrm{d}t'.$$
(16)

As shown in Eqs. (12) and (14) and approximation (16), the source power spectrum is related to the mean number of photoelectrons $\langle\langle N(t)\rangle\rangle$, the mean photocurrent $\langle\langle I(t)\rangle\rangle$, and the autocovariance matrix **K,** which are critical parameters for the computation of the detectability index and thus the AUC. Therefore the spectral characteristic of the light source employed is expected to strongly affect the performance of the Hotelling observer.

Having the mathematical expressions to compute the detectability index and AUC of the Hotelling observer, we need to model a sample to be employed in the imaging system, so the performance of the observer may be computed for a given task. In this investigation, we choose as a sample model a single layer, such as a glass plate, bounded by two different interfaces (A and B), as shown in Fig. 1. The first interface is assumed to be between air and the front surface of the sample that reflects a portion of the light beam, which is assumed to be normally incident upon the surface, because of the change in refractive index from 1 to n, where n is the refractive index in the sample. The second interface is modeled to be between the sample and a substrate with a refractive index given by $n + \Delta n$. The Fresnel reflection coeffi-

cients at the first and second interfaces at normal incidence are given by

$$r_1 = \frac{1 - n}{1 + n}, \qquad r_2 = \frac{-\Delta n}{2n + \Delta n}.$$
(17)

The more general expressions of the Fresnel coefficients would be used for nonnormal incidence.[15] With the thickness of the layer represented by a variable l, the phase accumulation of light propagating in the layer is given by $\exp(i\omega nml/c)$, where m is the number of passes through the layer and c is the speed of light in vacuum. Assuming the rest of the system as ideal, the frequency response of the sample arm $\hat{\alpha}_s(\omega)$ is given by the response of the modeled sample as

$$\hat{\alpha}_s(\omega) = r_1 + (1 - r_1^2)r_2 \exp\left(i\omega \frac{n2l}{c}\right),$$
(18)

where we assume that the reflected optical power becomes negligible for the second- and higher-order reflections at the interfaces, indicated by a dashed line in Fig. 1. We ignore the losses and phase shifts of the beam splitter. The reference mirror is assumed to have a flat reflection response with 100% reflectivity for all frequencies; $\hat{\alpha}_r(\omega)$ is 1.

5. Tasks

We focus this investigation on two classification tasks, a signal-detection task and a resolution task, for the performance assessment of the Hotelling observer in OCT imaging. These tasks are performed by the Hotelling observer, as described above, and the performance is evaluated by use of the detectability index and AUC analysis.

The signal-detection task is established to specify the minimum change in refractive index Δn between the sample layer and the substrate at the second interface, which can be detected by the system. The thickness of the layer l is set to a constant quantity that is approximately twice the source coherence length so that the light beams reflected from the first and second interfaces (A and B) of the sample do not interfere. If there is no second interface to be detected, then hypothesis H_0 is true. Under ideal conditions there is no second interface if Δn equals zero. On the other hand, the second interface can be detected, i.e., there is a second interface, for any Δn larger than zero. This is the case when hypothesis H_1 is true. The observer computes the detectability index and AUC as a function of Δn to determine how they behave with increasing values of Δn.

The goal of the resolution task is to assess the minimum thickness of the sample layer that the system can discriminate and to observe the performance of the observer with increasing thickness of the sample. We set the change in refractive index from the sample layer to the substrate Δn to various constant values. When the thickness of sample layer l equals zero, the second interface overlays the first interface. This is the true case for hypothesis H_0. On the other
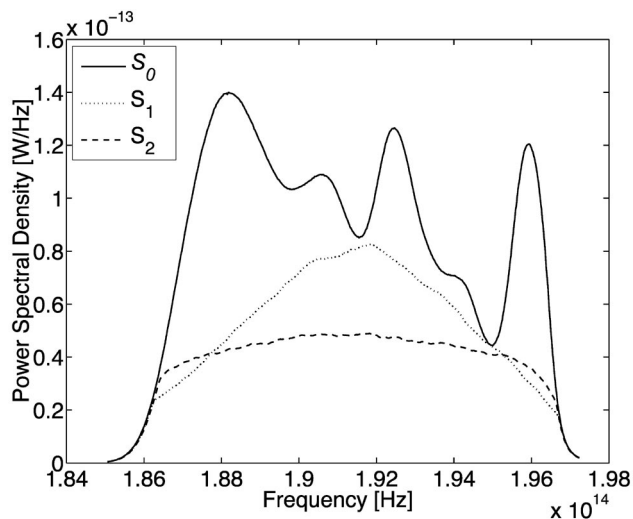
Fig. 2.   Solid curve, original power spectrum of the ASE source S_0; dotted curve, power spectrum after the first shaping operation S_1; dashed curve, power spectrum after the second shaping operation S_2.

hand, for a nonzero thickness l, hypothesis H_1 is true, that an interface may be resolved. The observer performance is quantified by computation of the detectability index and AUC as functions of the sample layer thickness l.

6. Simulation Results

We investigated the signal-detection and resolution tasks defined in the previous section while the Hotelling observer performed the task for different source power spectra. The first power spectrum we used in our simulation was that of a broadband amplified spontaneous emission (ASE) source (Newport BBS-430) emitting at 1565 ± 40 nm. Our goal is to compare the detectability index and AUC for un-shaped and shaped power spectra of the same ASE source. The shaping process was detailed in Ref. 4. We prepared the measured wavelength power spectra of the source before and after spectral shaping for simulations by first converting them to frequency spectra. The power spectra as functions of optical frequency were then normalized by the area under the original power spectrum, i.e., the source power before spectral shaping was performed. Figure 2 presents each power spectrum (S_0, the original source power spectrum; S_1 and S_2, shaped power spectra) prepared to be employed in the simulations. The original power spectrum of the ASE source contained significant spectral dips known to cause sidelobes in the point-spread function of the imaging system. With the spectral shaping process, smoother power spectra S_1 and S_2 with no spectral dips were created at the cost of 2.3 and 3.4 dB loss of optical power over the original power spectrum S_0, as shown in Ref. 4.

A. Signal-Detection Task

We previously described the signal-detection task and stated that it is performed to determine the effect
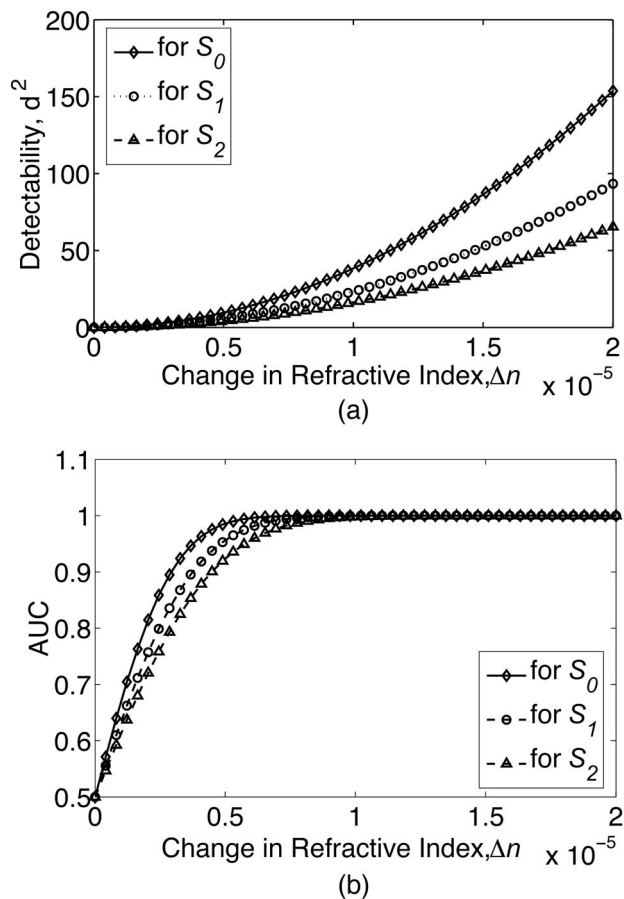

(a)

(b)

Fig. 3.   (a) Detectability and (b) AUC as a function of change in refractive index at the second interface.

of a change in refractive index Δn on the detectability index and AUC generated by the Hotelling observer, whereas the sample thickness l was set to a constant. We set the sample thickness l to 50 μm, which is approximately twice the longest coherence length computed for each power spectrum shown in Fig. 2.[4] In all simulations, the refractive index of the sample n, which was considered to be skin, was chosen to be 1.4. We simulated the detectability index as a function of a change in refractive index Δn and presented the results for each power spectrum in Fig. 3(a) as Δn was increased from zero to 2×10^{-5}. We then computed the AUC by using Eq. (5) and plotted the relation between the AUC and Δn in Fig. 3(b). We did not increase Δn beyond 2×10^{-5} because all AUC curves already reached their maximum, i.e., one, before Δn equals 2×10^{-5}. The value of the AUC corresponds to the probability of a correct classification in a two-alternative forced-choice test. For example, AUC equals one when the probability of correct classification of a detected signal is 100%. For AUC values of less than unity, for example, 0.75, the probability of correct classification is 75%, and there is also a 25% chance for the signal not to be classified correctly, i.e., as present, because the signal will be under the noise level 25% of the time.

Figure 3(a) shows that the detectability index for

the original power spectrum is larger than those for the two shaped power spectra for any nonzero Δn. The optical spectral shaping is based on attenuating the optical power at certain wavelengths, and thus it causes an inevitable power loss. Indeed, we see in Fig. 3(a) that the power spectrum that encloses larger optical power provides higher detectability index values at a given value of Δn when compared with the others. Furthermore, a detectability curve with a larger value than the others leads to an AUC curve that reaches its maximum, i.e., one, for smaller Δn, as shown in Fig. 3(b). At AUC equal to one, a smaller Δn ensures a smaller reflection coefficient given by Eqs. (17) and thus smaller reflectivity at the second interface, which is evaluated as the minimum reflectivity at the second interface, providing a correct classification of a present signal with 100% probability. The minimum reflectivity for 100% probability of correct classification of a present signal can be related to the concept of system sensitivity broadly published in the OCT literature.[11–13] When the three AUC curves in Fig. 3(b) are compared, it can be seen that the AUC curve for spectrum S_0 reaches one at Δn equal to 1.007×10^{-5}, whereas for S_1 and S_2 the corresponding values of Δn are 1.160×10^{-5} and 1.365×10^{-5}, respectively. Inserting those values of Δn into Eqs. (17) and computing the square of the reflection coefficient values with a sample refractive index n of 1.4 yields reflectivities of -108.9, -107.6, and -106.2 dB for a 100% probability of correct classification of a present signal for the sources with the power spectra S_0, S_1, and S_2, respectively, where 0 dB corresponds to 100% reflectivity.

To suppress the effect of difference in optical power in the simulation, we normalized each power spectrum individually with its optical power, i.e., the area under the measured power spectrum, so that each normalized power spectrum enclosed the same optical power, which is unity. For each power spectrum shown in Fig. 4(a), we present in Fig. 4(b) the AUC curves as functions of changes in the refractive index. Although the AUC curve for the original power spectrum is the same in Figs. 3(b) and 4(b), we observe that the AUC curves generated from power spectra with different spectral shapes but the same power overlap closely. Both simulations demonstrate that the optical power is the dominant parameter while simulating the detectability index and AUC for various changes in refractive index Δn in a detection task.

B. Resolution Task

The goal of the resolution task is to quantify the minimum sample thickness l for which the OCT system can resolve the reflections from interfaces A and B of the sample shown in Fig. 1. To study the performance of the Hotelling observer for the resolution task, we set Δn to certain constant values and vary the sample thickness l for each value of Δn. We used the information presented in Fig. 3(b) to select values of Δn. From Fig. 3(b), for each curve we selected the
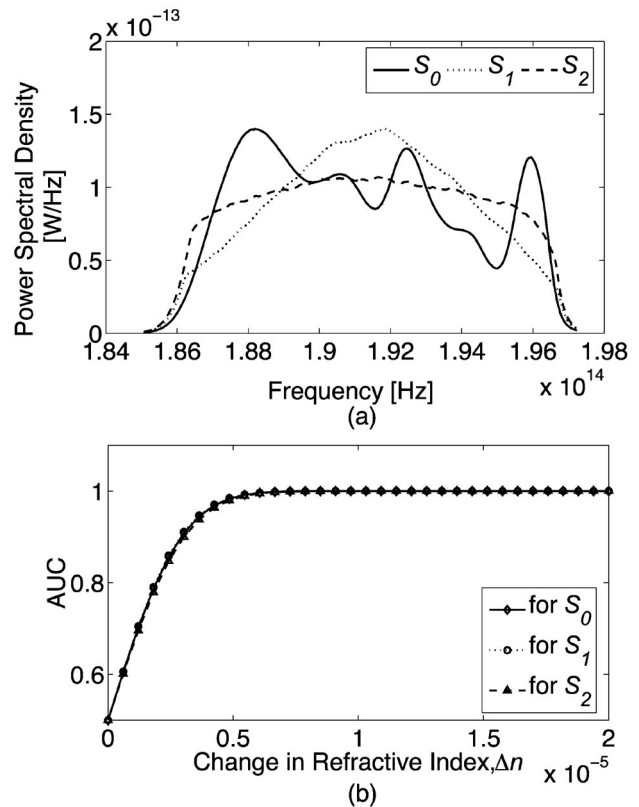

Fig. 4. (a) Power spectra each normalized to have unit power, (b) AUC as a function of change in refractive index for the power spectra shown in (a).

Δn, denoted as Δn_1, providing an AUC value of 0.75, and the minimum Δn, denoted as Δn_2, providing an AUC value of 1; we then doubled Δn_2, which is denoted as Δn_3.

To simulate the performance of the Hotelling observer for the resolution task, we determined Δn_1, Δn_2, and Δn_3 from Fig. 3(b) respectively as 1.543×10^{-6}, 1.007×10^{-5}, and 2.014×10^{-5} for the power spectrum S_0 in Fig. 2, 1.976×10^{-6}, 1.160×10^{-5}, and 2.320×10^{-5} for the power spectrum S_1 in Fig. 2, and 2.362×10^{-6}, 1.365×10^{-5}, and 2.730×10^{-5} for the power spectrum S_2 in Fig. 2. The detectability index and AUC as a function of the sample thickness l for each power spectrum and for each selected change in refractive index value are shown in Fig. 5.

In Figs. 5(a)–5(c) we observe that the detectability index for the resolution task increases with an increasing change in refractive index. The AUC curves shown in Figs. 5(d)–5(f), which equal 0.5 for zero sample thickness, i.e., two overlapping interfaces, reach the value of one faster for larger values of Δn. On the other hand, for all minimum changes in refractive index chosen Δn_1, the AUCs never reach one, which means that the probability of resolution for small changes in refractive index never becomes 100%. However, those AUC curves tend to approach an asymptote about an AUC value of 0.85. Until the asymptote is reached, we observe oscillations in AUC
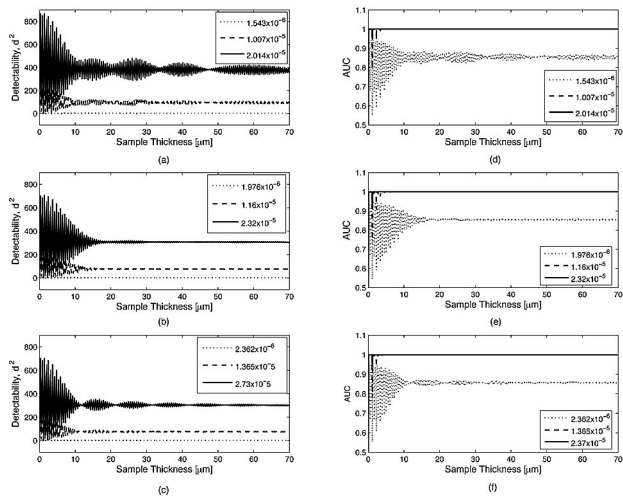
Fig. 5. Detectability index as a function of the sample thickness for the ASE source (a) with the power spectrum S_0, (b) with the shaped power spectrum S_1, and (c) with the shaped power spectrum S_2, and the corresponding AUC as a function of the sample thickness for the power spectra (d) S_0, (e) S_1, and (f) S_2.

curves as well as detectability index curves for sample thicknesses of less than half the coherence length of the source in the sample. The oscillation period is measured as half the center wavelength of the source, which is the period of the interference fringes for any broadband light source centered at the same wavelength. Thus the oscillations indicate that the light beam reflected from the first interface interferes with the one reflected from the second interface, if the sample thickness satisfies the condition that the light beam travels an optical path less than half the coherence length. The oscillations in the AUC of the sources represented with power spectra S_1 and S_2 show that the probability of discrimination of interfaces by the Hotelling observer fluctuates continuously over a broader range of sample thickness even if it is well above half the source coherence length in the sample.

7. Discussion

We have demonstrated the effect of the source spectral shape on the performance of the Hotelling observer derived for an OCT system and two tasks, a signal-detection task and a resolution task. The noise sources considered in the simulations are Gaussian noise from the broadband source and Poisson noise from the detector. Except for those sources of noise, the system is assumed to be ideal with unpolarized light, no dispersion in the sample and imaging system, and linear scanning of a homogeneous sample with normally incident light experiencing Fresnel reflections at the boundaries of the sample.

As a continuation of previous studies, in which the effect of spectral shape on the point-spread function and image of the OCT systems was discussed,[3,4] we show in this paper that the spectral shape is a major factor in the quantitative assessment of performance when a resolution task is considered. Our analysis

indicates that, for a signal-detection task, the area under the power spectrum curve, i.e., the optical power of the light source, is dominant and sources with higher power are expected to provide a larger detectability index, irrespective of their shape, and an associated AUC that increases faster with the same change in refractive index Δn and reaches one for smaller values of Δn. When we equalized the optical power of the light source under various shaping, results showed that the AUC for each power spectrum overlapped closely. This finding indicates that shaping the source power spectrum does not have an effect on the OCT performance for the signal-detection task we defined and that the optical power of the light source is the major factor defining the performance of the system for that task. As part of this investigation, the relation of the AUC to the concept of the system sensitivity was demonstrated in a signal-detection task.

The second set of simulations presented the performance of the Hotelling observer in the assessment of a resolution task. Results showed that spectral irregularities in the source power spectrum lead to fluctuations in the detectability index and AUC curves over a large range of sample thicknesses while the change in refractive index Δn is relatively small, e.g., 1.543×10^{-6}. For larger values of Δn, we observed that the detectability index as a function of the sample thickness had larger values and the AUC curves reached one for small values of sample thickness. This phenomenon means that the Hotelling observer can discriminate the interfaces for any nonzero distance between them if Δn has a relatively large value.[5] The AUC paradigm presented in this study is considered to utilize not only one optical coherence tomogram but a set of them at various noise instances to evaluate the signal detection, i.e., the layer is present or not, or distinguishability of interfaces, i.e., resolution of two successive layers, based on a statistical decision theory framework, in which classification is measured in a probability scale from 50% to 100%, as opposed to a binary scale.

8. Conclusion

This study has quantified the AUC performance of the Hotelling observer for the tasks of detection and resolution in OCT as a function of the spectral shape of the light source, the output optical power, as well as the sample optical characteristics, i.e., change in refractive index. Results show that spectral shaping leaves the AUC performance for a signal-detection task invariant for equal power of the light source, whereas it plays a role in the resolution task. Future work will include the investigation of the role of spectral shaping as well as other engineering parameters for both more complex and different tasks along with additional noise sources and different signal-detection schemes. In this study we considered that the sample had a simple structure with two layers, i.e., interfaces, to establish a benchmark performance for the Hotelling oberserver performing the two de-

fined tasks. Real biological samples may have many interfaces within the source coherence length; thus future studies will be extended to include more complex and multilayered models.

References

1. D. Huang, E. A. Swanson, C. P. Lin, J. S. Schuman, W. G. Stinson, W. Chang, M. R. Hee, T. Flotte, K. Gregory, C. A. Puliafito, and J. G. Fujimoto, "Optical coherence tomography," Science **254,** 1178–1181 (1991).
2. J. M. Schmitt, "Restoration of optical coherence images of living tissue using the clean algorithm," J. Biomed. Opt. **3,** 66–75 (1998).
3. C. Akcay, P. Parrein, and J. P. Rolland, "Estimation of longitudinal resolution in optical coherence imaging," Appl. Opt. **41,** 5256–5262 (2002).
4. A. C. Akcay, J. P. Rolland, and J. M. Eichenholz, "Spectral shaping to improve the point-spread function in optical coherence tomography," Opt. Lett. **28,** 1921–1923 (2003).
5. J. Rolland, J. O'Daniel, C. Akcay, T. Delemos, K. S. Lee, K. Cheong, E. Clarkson, R. Chakrabarti, and R. Ferris, "Task-based optimization and performance assessment in optical coherence imaging," J. Opt. Soc. Am. A **22,** 1132–1142 (2005).
6. H. H. Barrett, C. K. Abbey, and E. Clarkson, "Objective assessment of image quality. III. ROC metrics, ideal observers, and likelihood-generating functions," J. Opt. Soc. Am. A **15,** 1520–1535 (1998).
7. H. H. Barrett, "Objective assessment of image quality: effects of quantum noise and object variability," J. Opt. Soc. Am. A **7,** 1266–1278 (1990).
8. H. H. Barrett and K. J. Myers, *Foundations of Image Science,* B. E. A. Saleh, ed., Wiley Series on Pure and Applied Optics (Wiley, 2004), pp. 801–911.
9. R. D. Fiete, H. H. Barrett, W. E. Smith, and K. J. Myers, "Hotelling trace criterion and its correlation with human-observer performance," J. Opt. Soc. Am. A **4,** 945–953 (1987).
10. S. D. Wollenweber, B. M. W. Tsui, D. S. Lalush, E. C. Frey, K. J. LaCroix, and G. T. Gullberg, "Comparison of Hotelling observer models and human observers in defect detection from myocardial SPECT imaging," IEEE Trans. Nucl. Sci. **46,** 2098–2103 (1999).
11. A. G. Podoleanu, "Unbalanced versus balanced operation in an optical coherence tomography system," Appl. Opt. **39,** 173–182 (2000).
12. A. M. Rollins and J. A. Izatt, "Optimal interferometer designs for optical coherence tomography," Opt. Lett. **24,** 1484–1486 (1999).
13. A. M. Rollins and J. A. Izatt, "SNR analysis of conventional and optimal fiber-optic low-coherence interferometer topologies," in *Coherence Domain Optical Methods in Biomedical Science and Clinical Applications IV,* V. V. Tuchin, J. A. Izatt, and J. G. Fujimoto, eds., Proc. SPIE **3915,** 60–67 (2000).
14. J. W. Goodman, *Statistical Optics* (Wiley, 2000).
15. M. Born and E. Wolf, *Principles of Optics,* 7th ed. (Cambridge U. Press, 2002), pp. 42, 562.